World Academy of Science, Engineering and Technology
International Journal of Electrical and Computer Engineering
Vol:4, No:4, 2010

Solver for a Magnetic Equivalent Circuit and Modeling the Inrush Current of a 3-Phase Transformer

Markus G. Ortner, Christian Magele, and Klaus Krischan

***Abstract*—**Knowledge about the magnetic quantities in a magnetic circuit is always of great interest. On the one hand, this information is needed for the simulation of a transformer. On the other hand, parameter studies are more reliable, if the magnetic quantities are derived from a well established model. One possibility to model the 3-phase transformer is by using a magnetic equivalent circuit (MEC). Though this is a well known system, it is often not an easy task to set up such a model for a large number of lumped elements which additionally includes the nonlinear characteristic of the magnetic material. Here we show the setup of a solver for a MEC and the results of the calculation in comparison to measurements taken. The equations of the MEC are based on a rearranged system of the nodal analysis. Thus it is possible to achieve a minimum number of equations, and a clear and simple structure. Hence, it is uncomplicated in its handling and it supports the iteration process. Additional helpful tasks are implemented within the solver to enhance the performance. The electric circuit is described by an electric equivalent circuit (EEC). Our results for the 3-phase transformer demonstrate the computational efficiency of the solver, and show the benefit of the application of a MEC.

***Keywords*—**Inrush current, magnetic equivalent circuit, nonlinear behavior, transformer.

I. Introduction

THE characterization of transformers by using magnetic equivalent circuits (MEC) is incredibly interesting. It offers a significant gain of accuracy in comparison to empirical / analytical methods, while needing lower computational effort compared to the finite element method (FEM). The transformer is modeled by a nonlinear lumped element network to achieve good simulation results. The number of elements is low compared to FEM. Hence a MEC offers high simplicity and computational efficiency respectively. A model utilizing MEC could be used for controlling, for significance analysis, and dynamic calculations, if it had a fast working solver. The development of such a solver is challenging. It is affected by the software used and the processor speed. But it is particularly linked to the design of the solver, especially in the case of nonlinear networks. Thus the implementation must take into consideration the manipulation of nonlinear elements and the compactness of the algorithm. The larger the network the more important is a systematic approach to setting up the equations.

MEC was presented for time-efficient first estimations of the magnetic characteristics in [4, 6, 8]. It was mentioned as third method alongside the empirical / analytical method and FEM for design purposes [6, 8]. The electric circuit linked to the magnetic circuit is usually modeled by an electric equivalent circuit (EEC). Reference [1, 7] show calculations with separated equivalent circuits for the MEC and the EEC. Another possibility is the integration of the magnetic characteristic into the EEC by using nonlinear inductors [2, 5]. Network analysis has been established by using the nodal analysis [2, 5, 7, 10] or by the loop analysis respectively [3, 4, 8]. Regardless of the way the algorithm is implemented, results of dynamic calculations achieved by this method show quite a low error level compared to measurements [1, 2, 7, 8]. The error for inrush currents simulation is reported to be lower than 10% in [1].

The paper at hand describes the parts for implementing a solver to simulate the inrush current of a three-phase transformer. The solver is realized by separate circuits for the MEC and the EEC. The arithmetic equations of the MEC are established by the nodal analysis and deal with linear and nonlinear permeances. Hence this part must be solved iteratively, which is a point of interest. The EEC deals with the ordinary differential equations. A structured procedure to set up the equations is shown. This is necessary in order to handle the large number of elements used to model the transformer. The elements themselves hold the material characteristics and geometry information. The characteristics are measured with a permeance meter.

II. Solver implementation

A. Nodal Analysis

The MEC consists of $N + 1$ nodes and B branches. The graph is the collection of all branches and nodes. To setup the equations of the MEC the loop or the nodal analysis can be chosen respectively. The loop analysis leads to $B - N$ linearly

M. G. Ortner and K. Krischan are with the Institute for Electric Drives and Machines, Graz University of Technology, Kopernikusgasse 24, Graz 8010 Austria (phone: 0043-316-873-7246; fax: 0043-316-873-107246; e-mail: markus.ortner@TUGraz.at, klaus.krischan@TUGraz.at).

C. Magele is with the Institute for Fundamentals and Theory in Electrical Engineering , Graz University of Technology, Kopernikusgasse 24, Graz 8010 Austria (e-mail: Christian.magele@TUGraz.at).

independent equations. The nodal analysis requires *N* linearly independent equations. In this case the nodal analysis was chosen because it is easier to establish by using the incidence matrix, no tree must be found, and there is the possibility for a computer aided setup of this matrix [9, 11, 14].

B. The Elementary Branch

All different types of branches that occur in the MEC are represented by the elementary branch shown in fig. 1.

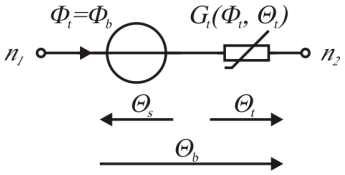

Fig. 1 The elementary branch consists of the magnetomotive force source Θ_s and the tube permeance G_t
Indexes: *b* … Branch, *s* … Source, *t* … Tube, *n* … Node

The value of the magnetomotive force (MMF) for the source Θ_s is nonzero for geometries which are surrounded or bordered by coils. For all other geometries Θ_s is zero. The tube permeance G_t is linear for geometries with linear material characteristics, i.e. air. G_t is nonlinear for geometries with nonlinear material characteristics and dependent on the magnetic tube flux Φ_t through G_t or the MMF for the tubes Θ_t of G_t respectively. The equations of the elementary branch are

$$\Theta_b = \Theta_t - \Theta_s \quad \Phi_b = \Phi_t \quad \Phi_t = G_t \cdot \Theta_t \,. \tag{1}$$

One can express G_t by using the relative permeance μ_r for a given flux density B_t or a magnetic field strength H_t and the normalized permeance $G_t^{'}$:

$$G_t = \mu_r\left(H_t, B_t\right) \cdot G_t^{'} \quad \text{with} \quad H_t = \Theta_t / L_t \quad \text{and} \quad B_t = \Phi_t / A_t \tag{2}$$

$G_t^{'}$ includes only the absolute permeability μ_0, the geometry data tube cross section area A_t, and tube length L_t.

$$G_t^{'} = \left(\mu_0 \cdot A_t\right) / L_t \tag{3}$$

C. Network Analysis

Furthermore vectors and matrices are marked with bold letters. Kirchhoff's current law in respect to the MEC denotes

$$\mathbf{A} \cdot \mathbf{\Phi}_b = \mathbf{0} \,. \tag{4}$$

The incidence matrix **A** contains the information about the network topology and $\mathbf{\Phi}_b$ is the flux branch vector. By using the branch and node relationship one can find

$$\begin{aligned} &\mathbf{\Phi}_t = \mathbf{Y}_t \cdot \mathbf{\Theta}_t \,, \quad \mathbf{\Theta}_t = \mathbf{A}^T \cdot \mathbf{\Theta}_n + \mathbf{\Theta}_s \quad \text{and} \quad \mathbf{Y}_n = \mathbf{A} \cdot \mathbf{Y}_t \cdot \mathbf{A}^T \\ &\Rightarrow \mathbf{Y}_n \cdot \mathbf{\Theta}_n = -\mathbf{A} \cdot \mathbf{Y}_t \cdot \mathbf{\Theta}_s = -\mathbf{A} \cdot \mathbf{\Phi}_s \end{aligned} \,. \tag{5}$$

The magnetic potentials of the nodes $\mathbf{\Theta}_n$ are related to **A** by $\mathbf{\Theta}_t$. The tube permeances $\mathbf{Y}_t$ consists of all $\mathbf{G}_t$. Because there are no coupled elements, $\mathbf{Y}_t$ is a diagonal matrix. Together with **A** the node permeance matrix $\mathbf{Y}_n$ can be calculated. The nodal analysis needs a flux source $\mathbf{\Phi}_s$. A single flux source can not be established. The whole flux of the source branch is denoted by $\mathbf{\Phi}$.

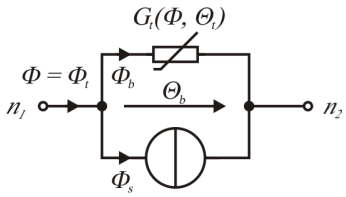

Fig. 2 The source branch which is necessary to fulfill the demands of the nodal analysis

One strategy for solving the source branch is to transform it into a MMF source with $\mathbf{\Theta}_s$. However, this transformation can not be computed directly, as $\mathbf{G}_t$ is dependent on the unknown parameters $\mathbf{\Phi}$ or $\mathbf{\Theta}_t$.

The second strategy is to split the entire network into two. The first network consists only of drain branches. These branches are made up of permeances only. With respect to the elementary branch, $\mathbf{\Theta}_s$ is zero. The network topology is summarized in $\mathbf{A}_d$. The second network consists of source branches only. Here $\mathbf{\Theta}_s$ is nonzero. This network topology is summarized in $\mathbf{A}_s$. One can write

$$\mathbf{Y}_d \cdot \mathbf{\Theta}_n + \mathbf{A}_s \cdot \mathbf{\Phi} = \mathbf{0} \quad \text{with} \quad \mathbf{Y}_d = \mathbf{A}_d \cdot \mathbf{Y}_t \cdot \mathbf{A}_d^T \,. \tag{6}$$

According to fig. 2 the fluxes of the source branch are defined as

$$\mathbf{\Phi} = \mathbf{\Phi}_b + \mathbf{\Phi}_s = \mathbf{G}_s \cdot \mathbf{A}_s^T \cdot \mathbf{\Theta}_n + \mathbf{w} \cdot \mathbf{G}_s \cdot \mathbf{i}_L \,. \tag{7}$$

By using this procedure it is possible to solve the nodal analysis with a minimum number of equations. The winding information **w** is included in (7), to express directly the coil-current $\mathbf{i}_L$ instead of $\mathbf{\Theta}_s$. These two equations written in matrix form lead to

$$\begin{bmatrix} \mathbf{Y}_d & \mathbf{0} \\ \mathbf{G}_s \cdot \mathbf{A}_s^T & \mathbf{G}_s \cdot \mathbf{w} \end{bmatrix} \cdot \begin{bmatrix} \mathbf{\Theta}_n \\ \mathbf{i}_L \end{bmatrix} = \begin{bmatrix} -\mathbf{A}_s \cdot \mathbf{\Phi} \\ \mathbf{\Phi} \end{bmatrix} . \tag{8}$$

The dimension of $\mathbf{Y}_d$ is *N* x *N*, and $\mathbf{A}_s$ is a *N* x *S* matrix, where *S* denotes the number of sources of the MEC. For solving (8) one condition has to be met: $\mathbf{A}_d$ must form a connected graph. In comparison, the tableau analysis shown in [9] leads to more equations than (8).

D. Time Domain

The EEC is established in the time domain. It consists of a source voltage *u*(*t*), an ohmic resistor R_{cu} for the copper resistance of the coil windings, an ohmic resistor R_{fe} for the iron losses, and an ohmic load resistor R_{load}. R_{cu}, and R_{load} are combined to the resistor R_{el}. The equations of the EEC are given by (9).

$$\mathbf{u}(t) = \mathbf{R}_{el} \cdot \mathbf{i}(t) + \mathbf{w} \cdot \dot{\mathbf{\Phi}}(t) \quad \text{with} \quad \mathbf{i}(t) = \mathbf{i}_L(t) + \mathbf{i}_{fe}(t) \tag{9}$$

The current **i**(t) is the sum of the currents $\mathbf{i}_L$ and $\mathbf{i}_{fe}$. $\mathbf{i}_{fe}$ denotes the current flowing through $\mathbf{R}_{fe}$, whereas $\mathbf{i}_L$ is responsible for $\mathbf{\Theta}_s$.

A constant time step Δt is chosen for the calculation. For every time step t_n the current $\mathbf{i}_L$ is found iteratively by the MEC, whereas $\mathbf{i}_{fe,n}$ is found with

$$\mathbf{i}_{fe,n} = \mathbf{w} \cdot \dot{\mathbf{\Phi}}_n \big/ \mathbf{R}_{fe} \,. \tag{10}$$

By rearranging (9) and inserting (10) into (9) one can find

$$\dot{\mathbf{\Phi}}_{n+1} = \mathbf{1}/\mathbf{w} \cdot \left[\mathbf{u}_n - \mathbf{R}_{el} \cdot \left(\mathbf{i}_{L,n} + \mathbf{w} \cdot \dot{\mathbf{\Phi}}_n / \mathbf{R}_{fe} \right) \right]. \quad (11)$$

E. Consideration of the Winding Connection

The windings of a transformer can be connected in delta or star. As only the line voltages are known from the measurement, (11) must be rearranged in the case of a star connection. This is done by using the connection matrix $\boldsymbol{M}_{conn}$, the condition matrix $\boldsymbol{M}_{cond}$, and the voltage matrices $\boldsymbol{M}_{vc}$ in accordance with [10]. For a three-phase star connected system these matrices are given without a detailed derivation by

$$\mathbf{M}_{conn} = \begin{bmatrix} 1 & -1 & 0 \\ 0 & 1 & -1 \end{bmatrix} \mathbf{M}_{cond} = \begin{bmatrix} 1 & 1 & 1 \end{bmatrix} \mathbf{M}_{vc} = \begin{bmatrix} 1 & 0 & 0 \\ 0 & 1 & 0 \end{bmatrix}. \quad (12)$$

Detailed information can be found in [10]. By inserting these matrices into (11) one will get

$$\mathbf{M}_{conn} \cdot \mathbf{w} \cdot \dot{\mathbf{\Phi}}_{n+1} = \mathbf{M}_{vc} \cdot \mathbf{u}_n - \mathbf{M}_{conn} \cdot \mathbf{R}_{el} \cdot \left(\mathbf{i}_{L,n} + \mathbf{w} \cdot \dot{\mathbf{\Phi}}_n / \mathbf{R}_{fe} \right). \quad (13)$$

Simplifying (13) and replacing the flux $\mathbf{\Phi}_n$ by the flux linkage $\mathbf{\Psi}_n$ leads to the ordinary differential equation (ODE) of the EEC.

$$\text{EEC:} \quad \boxed{\dot{\mathbf{\Psi}}_{n+1,conn} = \mathbf{u}_{n,vc} - \mathbf{R}_{conn} \cdot \left(\mathbf{i}_{L,n} + \dot{\mathbf{\Psi}}_n / \mathbf{R}_{fe} \right)} \quad (14)$$

This ODE is solved by an Euler approach. Hence, the flux of the next time step t_{n+1} is found with

$$\mathbf{\Psi}_{n+1,conn} = \mathbf{\Psi}_{n+1,conn} + \dot{\mathbf{\Psi}}_{n+1,conn} \cdot \Delta t \,. \quad (15)$$

Several different algorithms for integrating (15) in order to find $\mathbf{\Psi}_{n+1}$ are available. However, one must be aware that they need values of the estimated flux linkage $\mathbf{\Psi}^{i}_{n+1}$, which have to be found by using the iteration procedure of the MEC again.

F. Iteration Procedure

Considering $\mathbf{\Psi}_{conn}$, $\boldsymbol{M}_{cond}$, and the winding connection matrix

$$\mathbf{w}_{conn} = \mathbf{M}_{conn} \cdot \mathbf{w} \quad (16)$$

in (8), gives the equation system of the MEC.

$$\text{MEC:} \quad \boxed{\begin{bmatrix} \mathbf{Y}_n & \mathbf{A}_s \cdot \mathbf{G}_s \cdot \mathbf{w} \\ \mathbf{w}_{conn} \cdot \mathbf{G}_s \cdot \mathbf{A}_s^T & \mathbf{w}_{conn} \cdot \mathbf{G}_s \cdot \mathbf{w} \\ \mathbf{0} & \mathbf{M}_{cond} \end{bmatrix} \cdot \begin{bmatrix} \mathbf{\Theta}_n \\ \mathbf{i}_L \end{bmatrix} = \begin{bmatrix} \mathbf{0} \\ \mathbf{\Psi}_{conn} \\ \mathbf{0} \end{bmatrix}} \quad (17)$$

Below, the compact formulation of (17) is used with

$$\mathbf{T}(\mathbf{x}) \cdot \mathbf{x} = \mathbf{b} \,. \quad (18)$$

The dimension of the nonlinear matrix $\mathbf{T}$ is $N+S$. $\mathbf{T}$ includes all nonlinear and linear permeances. The solution vector $\mathbf{x}$ can be found for a given flux vector $\mathbf{b}$ by iteration. The iteration of the nonlinear equations of (18) can be performed using different procedures. Here, the direct iteration is applied. The advantage is the simplicity; the disadvantage is the high number of iterations required, especially for high saturation.

$$\mathbf{x}^{i+1} = \mathbf{T}^{-1}\left(\mathbf{x}^{i}\right) \cdot \mathbf{b} \quad (19)$$

The convergence tolerance ε denotes the difference of $\mathbf{G}_t$ between two iteration steps. It is chosen with 10^{-4}. The iteration procedure is drafted in fig. 3.

$$\mathbf{G}^{i}_{t,n} \rightarrow \left(\mathbf{T}^{i}\right)^{-1} \rightarrow \mathbf{x}^{i+1}_{n} \rightarrow \begin{matrix} \mathbf{\Theta}^{i+1}_{t,n} \\ \mathbf{\Phi}^{i+1}_{t,n} \end{matrix} \xrightarrow[data]{geometry} \begin{matrix} \mathbf{H}^{i+1}_{t,n} \\ \mathbf{B}^{i+1}_{t,n} \end{matrix} \rightarrow \mathbf{G}^{i+1}_{t,n}$$

Fig. 3 Iteration procedure

G. Permeance Extrapolation

After every time step the nonlinear permeances $\mathbf{G}_t$ are found by the iteration procedure. The number of iteration steps c_m strongly influences the computation time. One possibility to decrease c_m is the use of extrapolations of $\mathbf{G}_t$. The history of $\mathbf{G}_t(t)$ can be used in this way. Here, three types of extrapolation were investigated. The first applies a wraparound where the permeances $\mathbf{G}_t$ of the last time step are used as initial values for the iteration of the next time step. The second type is a linear extrapolation. Hence the last two time steps of $\mathbf{G}_t$ must be known. The third is a square extrapolation where the last three results of $\mathbf{G}_t$ must be recorded.

III. Application of the MEC and the EEC

A. Geometry of the Transformer

The three phase transformer consists of a core lamination and two hardboards on the upper and the lower yoke to compress the laminations. The material of the hardboard is steel. Coils are placed on every limb. The primary coil is on the inside, the secondary coil is wound around the outside. Both are star connected. A picture of this transformer can be seen in fig. 4. The main data are cited in the appendix.

Fig. 4 Transformer under investigation

B. Part Geometry

The basis of the MEC is the idea of flux tubes. The principles of flux tubes have been well described in the literature [6, 7, 10]. The flux tubes which represent volumes determine the flow direction and are defined by permeances within the MEC. Here, only rectangular flux tubes are used. The connected flux tubes define flux paths, which must be established during initialization. For a systematic approach, the shape of the transformer is separated into several components. Table I lists these components, the corresponding network

TABLE I
FLUX TUBE COMPONENTS AND THE CORRESPONDING MEC DATA

Component Name	Component Shape	Network Graph	Material
edge	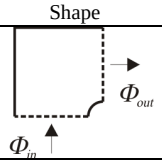	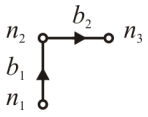	laminations, hardboard
yoke		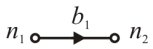	laminations/ hardboard
limb			lamination
air gap			air
tee	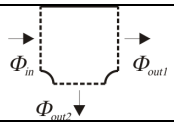	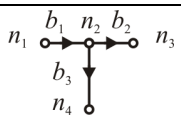	lamination hardboard
leakage	see (22)	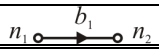	air

with the node and branch configuration, and the associated materials.

All branches listed in Table I are represented by the elementary branch in accordance with fig. 1. The normalized permeances G'_t are calculated with (3) by using the component geometries. The arrows of the figures in Table I indicate the predefined flux flow directions of the oriented branches. The non-magnetic paths of the overlapping areas within the edges and the places of joint are represented by an additional air gap δ. Hence, air gap and limb component are connected in series.

The permeances of the leakage path are estimated in accordance with [12]. For every coil, the leakage permeance G_σ is calculated by

$$G_\sigma = \frac{h_1 + 6\cdot h_2}{6\cdot b_w}\cdot l_1 + \frac{a_1 + 3\cdot a_2}{3\cdot h_1}\cdot l_2 . \qquad (20)$$

The total permeances of all coils are distributed homogenously across all leakage paths. The parameters in (20) are defined in the appendix.

C. Connected Network Graph

To create more detailed leakage paths and to situate the sources onto the limbs both the yokes and the limbs are segmented into two serial connected components. By connecting all the components listed in Table I, the MEC of the transformer is found. The connected graph is shown in fig. 5.

The laminations are displayed with solid lines, the hardboards with dashed lines, the air gaps with dotted lines, and the leakage paths with dash-dotted lines. The upper and the lower hardboards are both represented by one branch, because they have the same dimensions and material characteristics and effect in parallel to the yokes and edges. The components of each limb hold the MMF source of the primary and secondary coil. The connected graph consists of 30 nodes and 71 branches. To illustrate the connected and oriented graph in fig. 5 more clearly, the numbers of the nodes and branches are not included.

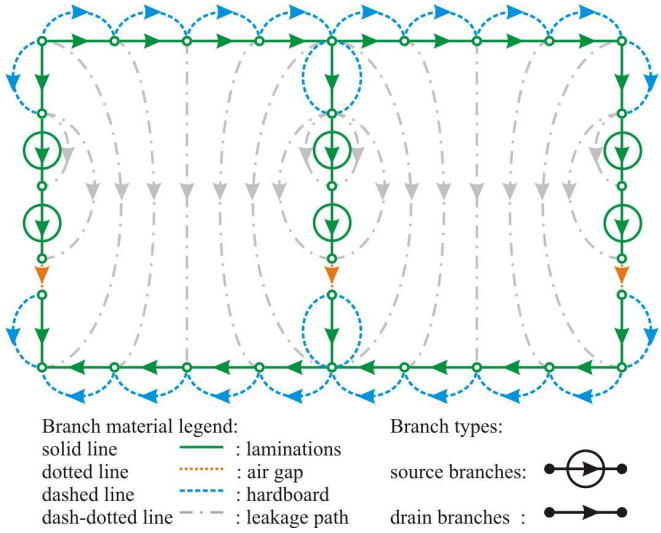

Fig. 5 Connected and oriented graph of the MEC for the three phase transformer

D. Material Characteristics

The BH curves of the laminations and the hardboard were measured in accordance with [15]. The init curve of both materials is shown in fig. 6. These curves are approximated by an analytical approach with exponential functions by

$$B(H) = \sum_{i=1}^{n} k_i \cdot \left(1 - e^{-H/k_{2i}}\right) + \mu_0 \cdot H . \qquad (21)$$

The init curve of the laminations is modeled with $n = 3$; for the hardboard $n = 2$ was sufficient. The measured curves and the resulting calculated curves can be seen in fig. 6.

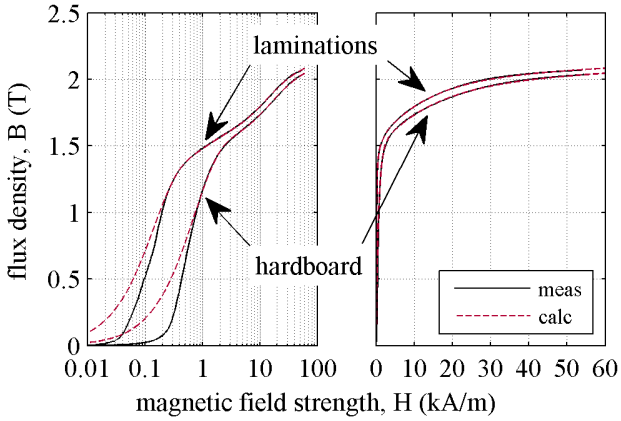

Fig. 6 Comparison of the measured and the calculated init curve of the laminations and the hardboard

The relative permeability μ_r is found by

$$\mu_r(H) = \frac{1}{\mu_0}\cdot\frac{B(H)}{H} = \frac{1}{\mu_0}\cdot\left(\sum_{i=1}^{n}\frac{k_i}{H}\cdot\left(1 - e^{-H/k_{2i}}\right) + \mu_0\right). \qquad (22)$$

The applied curve defined in (21) has a convex characteristic. Hence, for flux densities B lower than 1 T the magnetic field strength H of the calculated curve is lower than the measured H. On the other hand by using (21) the iteration process is stable and will converge [11]. For higher B the

measured and the calculated curves show almost the same values.

E. Indexing

The incidence matrix **A** is sparsely filled. It is used to calculate i.e. the drain permeance matrix $\mathbf{Y}_d$ in (6), (8), and in (17). Thus, it makes sense to ease the calculation effort. Table II shows an example for indexing the graph branches. The cited names are linked by numbers to the corresponding branches.

TABLE II
BRANCH CATEGORIES FOR THE INDEXING

Name	Category	Linearity	Sources
d	branches without sources	–	0
s	branches with sources	0	1
k	branches with nonlinear permeances	0	–
l	branches with linear permeances	1	0
m	branches without sources and with nonlinear permeances	0	0

Thus, sub matrices of the incidence matrix are found by applying the criteria of Table II. They use the mentioned name as subscript to the parameter. For example, the drain admittance matrix $\mathbf{Y}_d$ denotes to

$$\mathbf{Y}_d = \mathbf{A}_l \cdot \mathbf{Y}_t \cdot \mathbf{A}_l^T + \mathbf{A}_m \cdot \mathbf{Y}_t \cdot \mathbf{A}_m^T = \mathbf{Y}_l + \mathbf{Y}_m . \quad (23)$$

This matrix must be refreshed for every iteration step of every time step. By applying the indexing, only the m-Matrix must be refreshed. $\mathbf{Y}_l$ doesn't change throughout the entire simulation. Hence, it only needs to be calculated during the initialization. Since $\mathbf{A}_m$ is much smaller than **A** computation time is saved. Another example of the indexing is the replacement of a matrix multiplication. The process is drafted in (24). It leads to a vast reduction of computation. The parameter *n* holds the information of the appropriate node.

$$\mathbf{A}_{mY} = \mathbf{A}_m \cdot \mathbf{Y}_t \Rightarrow \mathbf{A}_{mY}(n,m) := \mathbf{Y}_t(m,m) \Rightarrow \mathbf{Y}_l = \mathbf{A}_{mY} \cdot \mathbf{A}_m^T \quad (24)$$

IV. RESULTS

A. Solver Handling

The calculation is separated into four parts. The first part is the initialization where the permeances $\mathbf{G}_t'$ are calculated from the geometries. Another task is the setup of the vectors for the magnetic and electric parameters, the setup of the network topology by means of the incidence matrix **A**, and extracting the categorized branch indexes, supporting the computational efficient algorithm described above (*E Indexing*). After this initialization, the iteration process for the MEC starts. This algorithm profits from a minimum number of equations by using the algorithm in (17) and a minimum number of calculation steps by applying the indexing. Then the results are fed into the EEC to calculate the ordinary differential equation of (14). Both the flux and the permeances are used in the next time step and its iteration process.

B. Inrush Current

Fig. 7 shows the measured and the calculated runs of the phase currents during the first three periods of the line voltage.

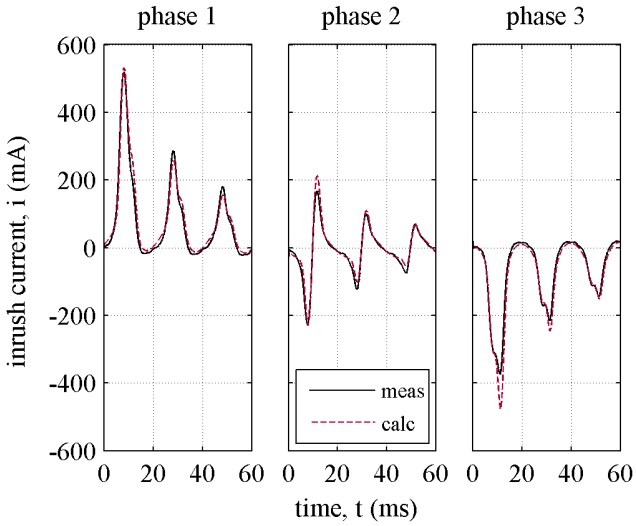

Fig. 7 Inrush current for all phases of the transformer

The line voltage on the primary windings was adjusted to 3x400 V@50 Hz. The phase currents and the line voltages of all phases of the transformer were recorded. Then, the recorded line voltages were used to feed the simulation model. The calculated phase currents are slightly higher for the first two periods. The deviation between calculation and measurement for the first maximum is in the range of ±5% for the first two phases, and ±20% for the third phase.

C. Steady State Current

After the decay of the transient effects, the steady state currents are available. For this transformer it takes about 3 s until steady state condition is reached. The measured and calculated runs of the phase currents are shown in fig. 8. For steady state condition the calculated current's amplitudes are slightly below the measured values.

The deviation for all phases is in the range of ±5%.

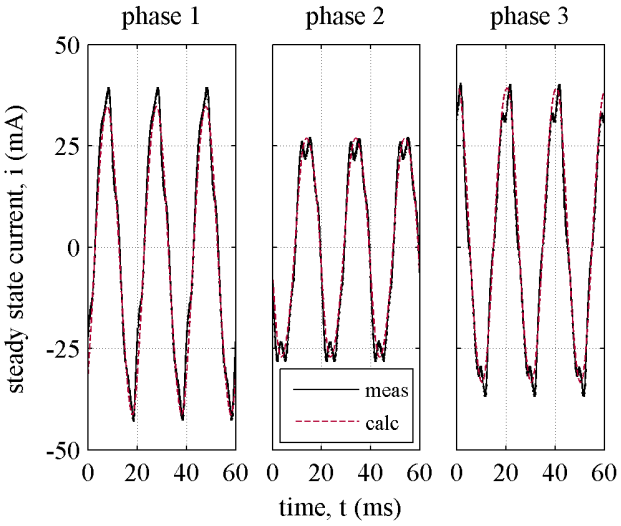

Fig. 8 Steady state current for all phases of the transformer

D. Flux in the Laminations and in the Hardboard

In fig. 9 both the magnetic flux in the laminations and in the hardboard is shown during inrush and steady state operation. The hardboard caries flux only for the first several periods. During this time the flux in the hardboard is close to 10% of the total flux.

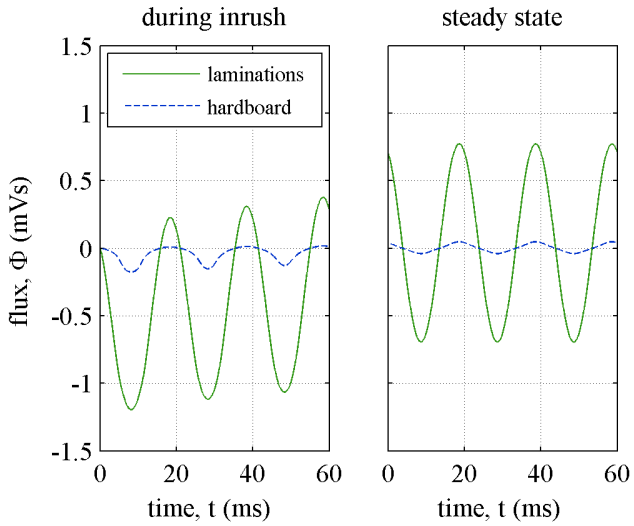

Fig. 9 Fluxes within the laminations and the hardboard during the transient and steady state respectively

Afterwards the share of the flux in the hardboard is about 3%. Hence, the hardboard offers an additional flux path during the transient time. If the hardboards are neglected in the MEC, the calculated inrush currents shown in fig. 7 will be about twice as high. Thus, the hardboards drastically reduce the maximum of the inrush currents.

E. Number of Iteration Steps

The number of iteration steps c_m depends on the used iteration process, and the degree of saturation. In this case the direct iteration is used. If there is strong saturation, c_m will be high. To decrease c_m the permeance extrapolation is applied. Fig. 10 compares the cumulative c_m for all investigated types of extrapolation.

The average number of iteration steps per time step can be found in Table III. It can be seen that the linear and the square extrapolation is very effective. The linear extrapolation has about 60%, and the square extrapolation has about 80% fewer iteration steps compared to the wraparound type. A well established permeance extrapolation is essential for an efficient calculation. The step size was chosen as 56 µs. The calculation time for one iteration accounted for about 600 µs on the computer used.

TABLE III
EFFECT OF PERMEANCE EXTRAPOLATION ONTO THE NUMBER OF ITERATIONS

Extrapolation type	Average number of iterations c_m
wraparound	7.2
linear	2.8
square	1.3

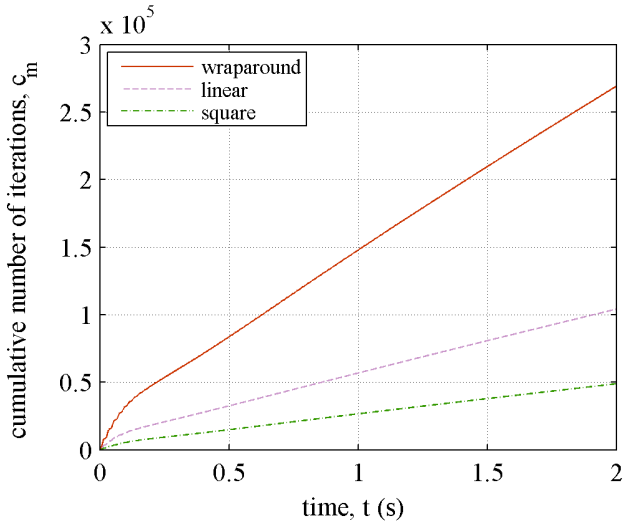

Fig. 10 Cumulative number of iteration steps by using different permeance extrapolations

V. DISCUSSION

The calculated current characteristics of all phases show good consistency to those measured. The current of the first phase shows a higher magnetization current compared to the third. This should be mainly affected by weaker laminations overlapping, which causes a higher equivalent air gap δ_u. The equivalent air gaps of the other two phases are smaller. The measured currents show harmonics which the calculated currents do not show, because of imperfections in modeling the BH curve. A remarkable flux through the hardboard occurs only during the first three periods. This is caused by the high excitation levels. After several periods the flux in the hardboard is almost negligible. Hence, the hardboard reduces the inrush current.

The Euler method for the integration algorithm is efficient enough because of small step size used. The used MEC is very detailed, thus it includes different flux paths. Every important part of the magnetic circuit is represented in the graph. The number of iteration steps can be reduced drastically by permeance extrapolation.

VI. CONCLUSION

The graph of the MEC is split into a drain and a source part. Hence, a minimum of equations must be solved for the nonlinear MEC by using the nodal analysis. This leads to a compact and fast solver. By establishing indexes for all characteristic branches of the graph, the solver is simple to handle. Hence, information about every branch can easily be found. A lot of preliminary work is carried out before the start of the simulation. This supports the calculation speed.

A satisfyingly good comparison between measurement and calculation is reached by this MEC and EEC. For most cases the difference between measurement and the calculation is in the range of ±10%.

VII. Appendix

Table IV lists the most important data of the transformer used. The type of the transformer is: FRITZCO DT 0.1/21.

TABLE IV
TRANSFORMER DATA

Parameter		Location	Value
nominal apparent power	S_N		95 VA
nominal frequency	f_N		50 Hz
nominal voltage	U_{1N}	primary	3 x 400 V
	U_{2N}	secondary	3 x 21 V
winding connection		primary	star
		secondary	star
windings	w_1	primary	1333
	w_2	secondary	122
ohmic resistance	R_{cu1}	primary	33.5 Ω
	R_{cu2}	secondary	0.665 Ω
wire diameter	d_{cu1}	primary	0.41 mm
	d_{cu2}	secondary	0.91 mm
iron loss resistance	R_{fe}		30 kΩ
yoke width	b_{yo}		22.5 mm
limb width	b_{li}		22.5 mm
hardboard width	b_{hb}		33.5 mm
window height	h_w		52.5 mm
window width	b_w		33.8 mm
laminations depth	t_L		33.0 mm
hardboard depth	t_{hb}		1.7 mm
coil height	h_1		46.3 mm
coil-yoke distance	h_2		3.1 mm
width coil	a_1	primary	6.6 mm
		secondary	3.2 mm
coil-limb distance	a_2	primary	2.0 mm
		secondary	8.5 mm
mean coil winding length within yoke	l_1	primary	38.3 mm
		secondary	48.1 mm
mean coil winding length without yoke	l_2	primary	114.8 mm
		secondary	144.2 mm
equivalent air gap	δ_u		0.03 mm
	δ_v		0.01 mm
	δ_w		0.01 mm

References

[1] S.G. Abdulsalam, W. Xu and V. Dinavahi, "Modelling and simulation of three-phase transformers for inrush current studies," *IEE Proc.-Gener. Transm. Distrib.*, vol. 152, No. 3, pp. 328-333, May 2005.

[2] J. Arrillaga, W. Enright, N.R. Watson and A.R. Wood, "Improved simulation of HVDC converter transformers in electromagnetic transient programs," *IEE Proc.-Gener. Transm. Distrib.*, vol. 144, No. 2, pp. 100-106, March 1997.

[3] A. Delale, L. Albert, L. Gerbaud and F. Wurtz, "Automatic generation of sizing models for the optimization of electromagnetic devices using reluctance networks," *IEEE Trans. Magn.*, vol. 40, No. 2, pp. 830-833, March 2004.

[4] J. Turowski, M. Turowski and M. Kopec, "Method of three-dimensional network solution of leakage field of three-phase transformers," *IEEE Trans. Magn.*, vol. 26, No. 5, pp. 2911-2919, September 1990.

[5] A. Medina and J. Arrillaga, "Simulation of multilimb power transformers in the harmonic domain," *IEE Proc.-C*, vol. 139, No. 3, pp. 269-276, May 1992.

[6] M. Amrhein and P.T. Krein, "Magnetic equivalent circuit simulations of electrical machines for design purposes," *IEEE Electric Ship Technologies Symposium, 2007*, pp. 254-260, May 2007.

[7] V. Ostović, "A method for evaluation of transient steady state performance in saturated squirrel cage induction machines," *IEEE Trans. Energy Conversion*, vol. EC-1, No. 3, pp. 190-197, September 1986.

[8] C.B. Rasmussen and E. Ritchie, "A equivalent circuit approach for predicting PM motor performance," *IEEE Ind. Applicat. Society Conference*, pp. 10-17, October 1997.

[9] L.O. Chua, C.A. Desoer and E.S. Kuh, "Linear and nonlinear Circuits," *McGraw-Hill series in electrical engineering*, Singapore: McGraw-Hill, 1987, pp. 214–232.

[10] V. Ostović, "Dynamics of saturated electric machines," New York: Springer Verlag New York, 1989, pp. 50–74, pp. 86–90, pp. 226–247.

[11] B. Peikari, "Fundamentals of network analysis and synthesis," in *Prentice-Hall network series*, New York: Prentice-Hall, 1974, pp. 91–147, pp. 303–314.

[12] H. Köfler, "Bemessung und Konstruktion elektrischer Maschinen," Graz: Institut für elektrische Antriebstechnik und Maschinen, 2007, pp. 71–72.

[13] J. Otto, "Berechnung linearer und nichtlinearer Netzwerke. Eine Einführung in die numerische Modellierung mit PSPICE," Leipzig, Köln: Fachbuchverlag Leipzig, 1994, pp. 42–49.

[14] R. Unbehauen, " Elektrische Netzwerke, Eine Einführung in die Analyse," 3. neu bearbeitete und erweiterte Auflage, Berlin: Springer Verlag, 1987, pp. 91–127.

[15] IEC 60404-4: 1995 + A1: 2000, Magnetic materials – Part 4: Methods of measurement of d.c. magnetic properties of magnetically soft materials.

Markus G. Ortner was born in Graz, Austria, in 1971. He attended the Graz University of Technology from 1992 to 1999, where he received a Dipl. Ing. degree from the Institute of Electrical Energy Innovations in 1999.

He worked as a project engineer with the same institute from 1999 to 2000, collaborating on the modeling of fuel cell systems. From 2000 to 2005 he worked as development engineer for EPCOS. He was responsible for modeling, and measurement of multilayer ceramic capacitors within high and low frequency respectively, and collaborated on the development of high frequency multilayer ceramic capacitors. Since 2005 he has been with the Institute of Electrical Drives and Machines. He is responsible for thermal measurements of electrical machines, and material measurements of magnetic material. His main field is modeling of magnetic circuits by using lumped elements. He is author of one, and coauthor of three scientific papers.

Christian Magele was born in Wolfsberg, Austria in 1960 and received the Ph.D. degree from the Graz University of Technology, Austria in 1991. Currently he is working as Associate Professor at the Institute for Fundamentals and Theory in Electrical Engineering at the Graz University of Technology, Austria.
His research interest include the development and application of optimization/identification methods coupled to numerical methods for the solution of electromagnetic field problems and the design of Web based courses for distant education.

Klaus Krischan was born in Leibnitz, Austria in 1965. He received the Dipl. Ing. and PhD in electrical engineering from the Graz University of Technology in 1990 and 1995, respectively. Since 1991 he has been working at the Institute for Electrical Drives and Machines of the Graz University of Technology where he has been Assistant Professor since 2001. His research concerns electrical drives and power converters.